CHAPTER 5

Dust scattering in the Galaxy: a case study of Orion

The main source of far-ultraviolet (FUV) diffuse emission in Orion is starlight coming from the Trapezium cluster at its center which gets scattered by dust in front of the nebula. In this chapter, we start by studying correlations between the FUV and infrared (IR) emissions in order to determine the types of dust contributing at our observed locations. We then use an existing model for studying the FUV dust scattering in Orion to check if it can be extended to regions away from the center in a 10 degree radius. Our dust model constrains the dust optical properties, albedo (α) and scattering phase function asymmetry factor (g), on different sides of the central Orion region. We have tried to investigate the variation of dust grain properties as one moves further away from the center of the Orion nebula.

5.1 Introduction and Motivation

The Orion Nebula (M42 or NGC 1976) is one of the most studied and nearest sites of active star formation in the Milky Way (MW) Galaxy [171]. It spans more than 700 deg^2 in the sky [74] with emissions at different wavelengths. M42 is one of the brightest sources in the ultraviolet (UV) sky [172] and is one of the first objects targeted with new instruments for calibration purposes. The dust properties in Orion are known to be different from average Milky Way dust with the presence of much larger dust grains [1]. The brightness in Orion is attributed to the light from the Trapezium cluster of stars being forward scattered by the thin sheet of neutral hydrogen (HI), known as Orion's veil [173, 174], located $\sim$1 pc in front of the nebula. The veil subtends an angle of at least $10'$ in the plane of the sky, which amounts to 1.5 pc at a distance of 500 pc [175] from us. An extensive review of the Orion nebula and related observations has been presented by O'Dell (2001) [176].

Murthy & Sahnow (2004) [110] reported the first far-ultraviolet (FUV) diffuse observations in this region with data from the *Far Ultraviolet Spectroscopic*

Explorer (FUSE) telescope. Shalima et al. (2006) [89] continued this work by modelling these observations to study the dust properties and found that the albedo of these grains varies from 0.3±0.1 at 912 Å to 0.5±0.2 at 1020 Å. The results of their proposed model were consistent with those of Draine (2003) [1]. In the recent past, a lot of work has been done to study the dust properties in the central region of Orion, mainly concentrating on the $\sim 5'$ diameter optically bright region referred to as the Huygens region [177] centered on the Trapezium stars, and the veil [74, 178–181], but studies on the surroundings of Orion have been limited.

In this work, we present the findings after applying the dust model used successfully by Shalima et al. (2006) [89] at the Orion center, to the surroundings of Orion in an unprecedented 10 degree radius. We have used archival data from the *Galaxy Evolution Explorer (GALEX)* [182] and from the *AKARI* space telescope [129] archives for this study. First, we present the correlations between the *GALEX* far-UV and the *AKARI* far-IR observations. We then proceed to model the dust scattered FUV light in the Orion surroundings which will tell us about the scattering properties of the dust grains (albedo, cross-section and scattering phase function), and the nature of dust species as we move away from the center of the nebula. We finally compare our results with previous work done for the Orion region and present our conclusions.

5.2 Sample of Observations

We have taken the location observed by Shalima et al. (2006) [89] as center, i.e. (l = 208.8, b = –19.3) in galactic coordinates, and looked for *GALEX* observations in a 10 degree radius. *GALEX* observed the ultraviolet (UV) sky in two wavelength bands: far-UV ($\lambda_{eff} \sim 1528$ Å, 1344–1786 Å) and near-UV ($\lambda_{eff} \sim 2310$ Å, 1771–2831 Å) [71, 72]. The details of the *GALEX* mission and telescope detectors have been discussed in Section 1.2.1. The *GALEX* all-sky imaging survey: AIS was completed in 2007 covering an area ∼26,000 deg^2 [74]. Since Orion is very bright in the UV, *GALEX* didn't observe the central region of the nebula due to instrumental constraints and the observations start from an angular distance of 6.96 degrees, which works to our advantage. We have an opportunity to apply a model working at the central region towards the outskirts of the nebula. We have taken 42 locations observed by *GALEX* in the FUV (1539 Å) from the final data release of the spacecraft (GR6/GR7). We have 40 observations from *GALEX* AIS and 2 observations from *GALEX* Guest Investigator (GI) program.

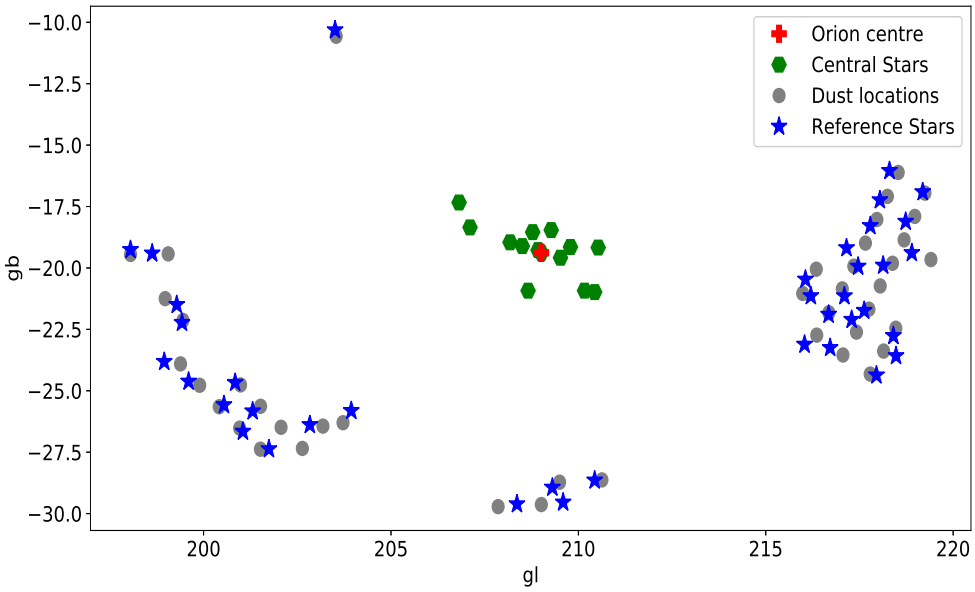

Figure 5.1: Our 42 locations around the Orion center. We have distributed the locations into four groups based on their position with respect to the center. The reference stars are used to get an estimate of the extinction and hydrogen column density near our dust locations with changing distance.

We have looked for infrared (IR) data at the same 42 locations in the *AKARI* legacy archive at four wavelength bands: 65 μm, 90 μm, 140 μm and 160 μm. These four wavelength bands were observed by the *AKARI* Far-Infrared Surveyor (FIS) [79] which was the instrument chiefly intended to make an all-sky survey at far-infrared wavelengths [80, 81]. The *AKARI* instrument details have been discussed in Section 1.2.1. Figure 5.1 shows our observed dust locations with respect to the Orion center.

5.3 Dust scattering model

We have used the model by Shalima et al. (2006) [89] and we try to constrain the albedo (α) and the asymmetry factor (g) of dust grains in the region surrounding Orion. The model uses the Henyey–Greenstein scattering phase function [90] as discussed in Section 1.3.3. The Trapezium cluster of stars in Orion is the brightest source of radiation from the nebula. But since our region under consideration is much further away from the center of M42, we have taken into account the 14 brightest stars, in addition to the Trapezium stars, as contributors of radiation at our locations as shown in Table 5.1.

Table 5.1: Properties of the 14 contributing central stars. The spectral type has been obtained from the SIMBAD astronomical database. The distance has been taken from the Hipparcos catalogue.

HD number	l (^{0})	b (^{0})	Spectral type	Distance (pc)	Luminosity (1539 Å) (ph cm^{-2} sec^{-1} sr^{-1} Å^{-1})	N(H) (cm^{-2})
037043	209.5221	-19.5835	O9III	406.5041	07.453 $\times 10^9$	11.870$\times 10^{21}$
037022	209.0107	-19.3840	O7V	450.4504	75.244 $\times 10^9$	342.245$\times 10^{21}$
036512	210.4356	-20.9830	O9.7V	473.9337	09.443 $\times 10^8$	1.906$\times 10^{21}$
037017	208.1770	-18.9571	B1.5V	373.1343	09.068 $\times 10^7$	6.508$\times 10^{21}$
037481	210.5290	-19.1698	B2IV/V	480.7692	08.111 $\times 10^8$	8.952$\times 10^{21}$
037303	209.7887	-19.1469	B2V	416.6667	02.842 $\times 10^8$	4.414$\times 10^{21}$
037061	208.9248	-19.2736	O9V	361.0108	02.098 $\times 10^9$	230.939$\times 10^{21}$
037018	208.5036	-19.1092	B1V	240.9639	02.352 $\times 10^9$	35.432$\times 10^{21}$
037356	208.7804	-18.5426	B3V	343.6426	02.753 $\times 10^8$	0.791$\times 10^{21}$
037526	209.2749	-18.4597	B5V	332.2259	06.272 $\times 10^6$	1.715$\times 10^{21}$
036487	210.1646	-20.9242	B6IV	377.3585	04.621 $\times 10^6$	1.328$\times 10^{21}$
037468	206.8163	-17.3360	O9.5V	352.1127	01.121 $\times 10^9$	2.317$\times 10^{21}$
037056	207.1087	-18.3495	B8/9V	446.4286	05.391 $\times 10^6$	2.883$\times 10^{21}$
036120	208.6580	-20.9250	B8V	390.6250	00.985 $\times 10^6$	0.527$\times 10^{21}$

The stellar luminosities as shown in Table 5.1 have been calculated using data from the *International Ultraviolet Explorer (IUE)* archives at 1539 Å. We have first used the all-sky 100 μm dust emission maps [111] to extract the E(B-V) for our stars. We have then used the dust cross-section per hydrogen atom from Draine (2003) [1] and an extinction R_v=5.5 for Orion to calculate the total extinction A(V) and hydrogen column density N(H) for each location:

$$\frac{A(V)}{E(B-V)} = R(V) = 5.5 \tag{5.1}$$

$$\frac{N(H)}{A(V)} = 1.8 \times 10^{21} \ atoms\ cm^{-2}\ mag^{-1} \tag{5.2}$$

Since we do have much idea about the dust properties at our 42 locations, we have selected a set of reference stars as shown in Figure 5.1 from the Hipparcos catalogue [183] close to the dust in order to get a better estimate of the extinction and distance to our locations. We use a CO map from *Planck* telescope archive [184] to separate the molecular component, N(CO) from the total N(H). Now, the E(B-V) values of the stars differ with distance: very close to the center the dust density is high, so we make a table of N(H) values for these stars and put them in bins of suitable size to allow us to compare with the values at these locations.

In our dust model, we only consider single-scattering due to the presence of Orion's Veil in front of the nebula which scatters the light from the 14 stars we have considered. We mainly put the N(H) values in front of the reference stars. The optical depth is given as, $\tau(\lambda) = N(H) \times \sigma$, where λ=1539 Å and σ is the extinction cross-section. Since we have low values of τ ($\ll$1), single-scattering dominates. Hence, the reference stars in Figure 5.1 are used for distributing the material. If we see the column density remaining constant despite the distance, then we put the entire N(H)–N(CO) in front of the star. Otherwise, we put two or three sheets of 0.1 pc so that we get the total column density. For example, N(H)=4.6e21 is in front of the reference star. So we put 4.6e21/(3e18×0.1) at 210 pc and (6.69e21–4.6e21)/(3e18×0.1) at 450 pc, where 6.69e21 is the total N(H) for the dust location. Dividing N(H) by the factor (3e18×0.1) gives us the number density of hydrogen atoms. Hence, if the column density is same with distance, then all the dust is in front of the closer reference star. Assuming the same 'α' and 'g' throughout and varying the distance and column densities, we try to get a good fit between the *GALEX* FUV observations and our model output which will give us the 3D dust distribution as well.

5.4 Data analysis and Results

Using aperture photometry technique as discussed in Section 1.3.1, we have calculated the FUV and FIR intensities from the *GALEX* and *AKARI* archival data. The observed *GALEX* FUV intensities have been corrected for airglow and background emission as described by Murthy (2014) [75]. The FUV intensities along with the *GALEX* observation details are shown in Table 5.2. Similarly, the FIR intensities have been calculated using *AKARI* FIS archival data which has already been corrected for background contamination [81]. The FIR intensities at our dust locations are shown in Table 5.3 as $I_{65\mu m}$, $I_{90\mu m}$, $I_{140\mu m}$ and $I_{160\mu m}$ where the subscript represents the wavelength in microns as observed by *AKARI*.

Table 5.2: Details of *GALEX* FUV observations around Orion.

Survey	l (^{0})	b (^{0})	Angular distance (degrees)	Exp. time (sec)	FUV intensity (1539 Å) (ph cm^{-2} sec^{-1} sr^{-1} $Å^{-1}$)
AIS	215.9858	-21.03678	6.96443	216	13192.089 ± 43.425
AIS	216.3477	-20.05170	7.14608	247	11670.878 ± 38.819
AIS	216.6843	-21.82404	7.80018	104	10691.843 ± 55.926
AIS	216.3610	-22.73478	7.84751	213	9540.414 ± 14.409
AIS	217.0416	-20.85384	7.89419	390.15	10889.231 ± 135.868
AIS	217.3502	-19.92887	8.07774	198	9935.189 ± 61.848
AIS	217.6604	-18.98852	8.37539	190	9244.332 ± 17.995
GI	203.7195	-26.30023	8.41982	1654.15	7533.637 ± 27.338
AIS	217.4199	-22.61161	8.70199	186	9441.720 ± 29.970
AIS	217.7529	-21.67958	8.71578	211.05	10264.169 ± 4.507
AIS	217.9658	-18.02852	8.77530	199	10691.843 ± 10.494
AIS	217.0605	-23.54354	8.78004	191.1	10428.659 ± 59.874
AIS	218.0538	-20.73285	8.81077	199	11514.293 ± 30.233
AIS	203.1845	-26.43842	8.81313	169	6448.004 ± 22.732
AIS	218.3820	-19.80989	9.04263	136	10264.169 ± 76.981
AIS	200.9855	-24.76113	9.06785	176	10922.129 ± 22.765
AIS	199.4499	-22.13578	9.19124	112	10527.353 ± 107.905
AIS	199.0548	-19.42800	9.19351	181.05	13257.885 ± 68.427
AIS	201.5206	-25.63027	9.23280	188	8158.699 ± 15.560
AIS	218.2467	-17.08630	9.24187	194	10461.557 ± 26.219
AIS	218.6914	-18.85640	9.35742	217	10000.985 ± 19.640
AIS	198.9741	-21.24889	9.41884	110	10922.129 ± 196.400
AIS	209.4986	-28.72108	9.44258	283	9507.516 ± 45.728
AIS	210.6291	-28.62830	9.47636	168	9672.006 ± 38.819
AIS	202.0663	-26.48617	9.48874	184.05	5329.472 ± 34.213
AIS	218.4705	-22.45449	9.56769	265	8356.086 ± 52.636
AIS	218.1448	-23.38423	9.61104	204.05	8520.576 ± 13.619
AIS	217.7865	-24.31932	9.73240	201.05	8685.066 ± 6.941
AIS	218.9770	-17.90198	9.74467	213.1	10264.169 ± 60.532
AIS	218.5336	-16.11330	9.80239	197	10264.169 ± 38.819
AIS	202.6347	-27.34658	9.83424	189	6119.024 ± 44.083
AIS	199.3837	-23.90570	9.88809	174	10362.863 ± 66.124
AIS	199.8962	-24.77457	9.89899	184.05	12468.334 ± 246.734
AIS	219.4075	-19.65953	10.00526	220	9704.904 ± 55.597
AIS	200.4167	-25.65025	10.01125	185	5921.636 ± 69.414
GI	203.5377	-10.56900	10.10049	2446.25	17008.255 ± 103.957
AIS	198.0511	-19.44966	10.13952	192	14244.825 ± 106.589
AIS	219.2478	-16.95318	10.20073	273	11185.313 ± 34.542
AIS	200.9614	-26.51945	10.20460	187	5822.942 ± 2.957
AIS	209.0111	-29.63168	10.33346	288.05	10033.883 ± 248.708
AIS	207.8586	-29.71661	10.45161	296	6119.024 ± 28.851
AIS	201.5159	-27.37775	10.48114	188	5066.288 ± 57.242

Table 5.3: Details of *AKARI* FIR observations around Orion.

l (^{0})	b (^{0})	$I_{65\mu m}$ (MJy sr^{-1})	$I_{90\mu m}$ (MJy sr^{-1})	$I_{140\mu m}$ (MJy sr^{-1})	$I_{160\mu m}$ (MJy sr^{-1})
215.9858	-21.03678	7.406 ± 2.554	5.720 ± 0.728	104.965 ± 65.045	19.430 ± 4.645
216.3477	-20.05170	5.016 ± 1.697	6.939 ± 0.437	15.441 ± 0.788	24.855 ± 5.945
216.6843	-21.82404	1.679 ± 1.179	5.685 ± 0.494	16.532 ± 0.979	15.916 ± 0.651
216.3610	-22.73478	1.962 ± 1.694	5.385 ± 0.233	17.261 ± 1.726	18.142 ± 3.573
217.0416	-20.85384	1.914 ± 1.931	4.932 ± 0.324	11.089 ± 0.763	14.551 ± 3.319
217.3502	-19.92887	0.925 ± 2.111	6.476 ± 0.965	13.311 ± 1.801	16.783 ± 5.309
217.6604	-18.98852	3.018 ± 2.392	5.147 ± 0.247	16.001 ± 0.735	17.148 ± 2.031
203.7195	-26.30023	6.525 ± 2.755	9.778 ± 4.350	13.059 ± 3.042	10.379 ± 5.982
217.4199	-22.61161	3.875 ± 1.866	5.337 ± 0.273	18.672 ± 1.157	16.480 ± 0.652
217.7529	-21.67958	6.643 ± 1.358	5.168 ± 2.467	6.064 ± 0.367	9.464 ± 5.861
217.9658	-18.02852	5.347 ± 0.815	11.691 ± 0.478	41.122 ± 1.037	37.812 ± 3.314
217.0605	-23.54354	5.202 ± 2.196	8.678 ± 0.295	21.808 ± 0.946	18.154 ± 5.948
218.0538	-20.73285	3.158 ± 0.680	6.768 ± 0.355	17.483 ± 0.956	15.739 ± 2.787
203.1845	-26.43842	2.710 ± 1.774	2.143 ± 0.280	6.151 ± 0.280	6.563 ± 1.035
218.3820	-19.80989	3.828 ± 2.425	4.938 ± 0.319	14.072 ± 1.020	11.541 ± 2.761
200.9855	-24.76113	3.615 ± 1.771	4.406 ± 0.330	8.334 ± 0.391	8.891 ± 0.998
199.4499	-22.13578	3.685 ± 2.715	3.687 ± 0.458	8.420 ± 0.097	6.484 ± 1.966
199.0548	-19.42800	4.226 ± 1.688	5.250 ± 0.411	10.893 ± 1.502	10.694 ± 2.178
201.5206	-25.63027	1.672 ± 2.761	2.947 ± 0.421	5.884 ± 0.491	7.373 ± 1.816
218.2467	-17.08630	4.712 ± 2.117	6.440 ± 0.341	16.650 ± 1.496	18.540 ± 7.587
218.6914	-18.85640	3.415 ± 1.235	6.217 ± 0.482	17.582 ± 0.478	17.372 ± 2.266
198.9741	-21.24889	1.623 ± 2.254	4.448 ± 0.463	8.919 ± 0.600	10.488 ± 1.734
209.4986	-28.72108	3.653 ± 1.743	4.990 ± 0.287	9.750 ± 0.624	14.427 ± 3.743
210.6291	-28.62830	4.826 ± 2.098	4.961 ± 0.434	12.482 ± 1.063	9.541 ± 3.260
202.0663	-26.48617	3.252 ± 1.880	2.550 ± 0.455	5.799 ± 0.815	6.197 ± 2.183
218.4705	-22.45449	1.034 ± 2.694	4.438 ± 0.342	9.545 ± 0.448	7.608 ± 3.438
218.1448	-23.38423	2.323 ± 1.931	4.819 ± 0.562	13.581 ± 0.697	19.994 ± 13.181
217.7865	-24.31932	2.661 ± 1.174	4.486 ± 0.378	9.728 ± 0.433	7.484 ± 1.591
218.9770	-17.90198	2.768 ± 1.656	8.024 ± 0.545	21.128 ± 1.697	21.301 ± 4.265
218.5336	-16.11330	5.729 ± 1.934	8.196 ± 0.364	27.330 ± 1.727	19.215 ± 3.904
202.6347	-27.34658	3.723 ± 2.174	2.328 ± 0.335	4.282 ± 0.399	7.278 ± 3.074
199.3837	-23.90570	2.510 ± 1.028	4.815 ± 0.487	6.580 ± 0.918	8.053 ± 0.769
199.8962	-24.77457	4.398 ± 3.124	5.288 ± 0.361	10.406 ± 0.718	7.349 ± 5.469
219.4075	-19.65953	5.010 ± 0.809	5.855 ± 0.233	16.949 ± 0.970	15.977 ± 1.486
200.4167	-25.65025	3.042 ± 1.296	3.026 ± 0.355	6.915 ± 0.239	8.119 ± 2.381
203.5377	-10.56900	6.065 ± 2.582	15.911 ± 0.571	42.355 ± 2.233	43.627 ± 4.707
198.0511	-19.44966	2.064 ± 1.822	4.814 ± 0.424	9.527 ± 0.924	7.729 ± 2.922
219.2478	-16.95318	4.141 ± 2.184	7.472 ± 0.368	20.543 ± 1.221	13.462 ± 3.116
200.9614	-26.51945	5.263 ± 2.166	2.411 ± 0.250	5.872 ± 0.450	6.565 ± 1.233
209.0111	-29.63168	4.545 ± 2.201	5.229 ± 0.436	11.048 ± 0.372	9.767 ± 1.216
207.8586	-29.71661	4.195 ± 1.992	2.940 ± 0.386	6.128 ± 1.154	7.132 ± 0.605
201.5159	-27.37775	3.229 ± 2.758	2.214 ± 0.472	4.830 ± 0.380	12.611 ± 10.570

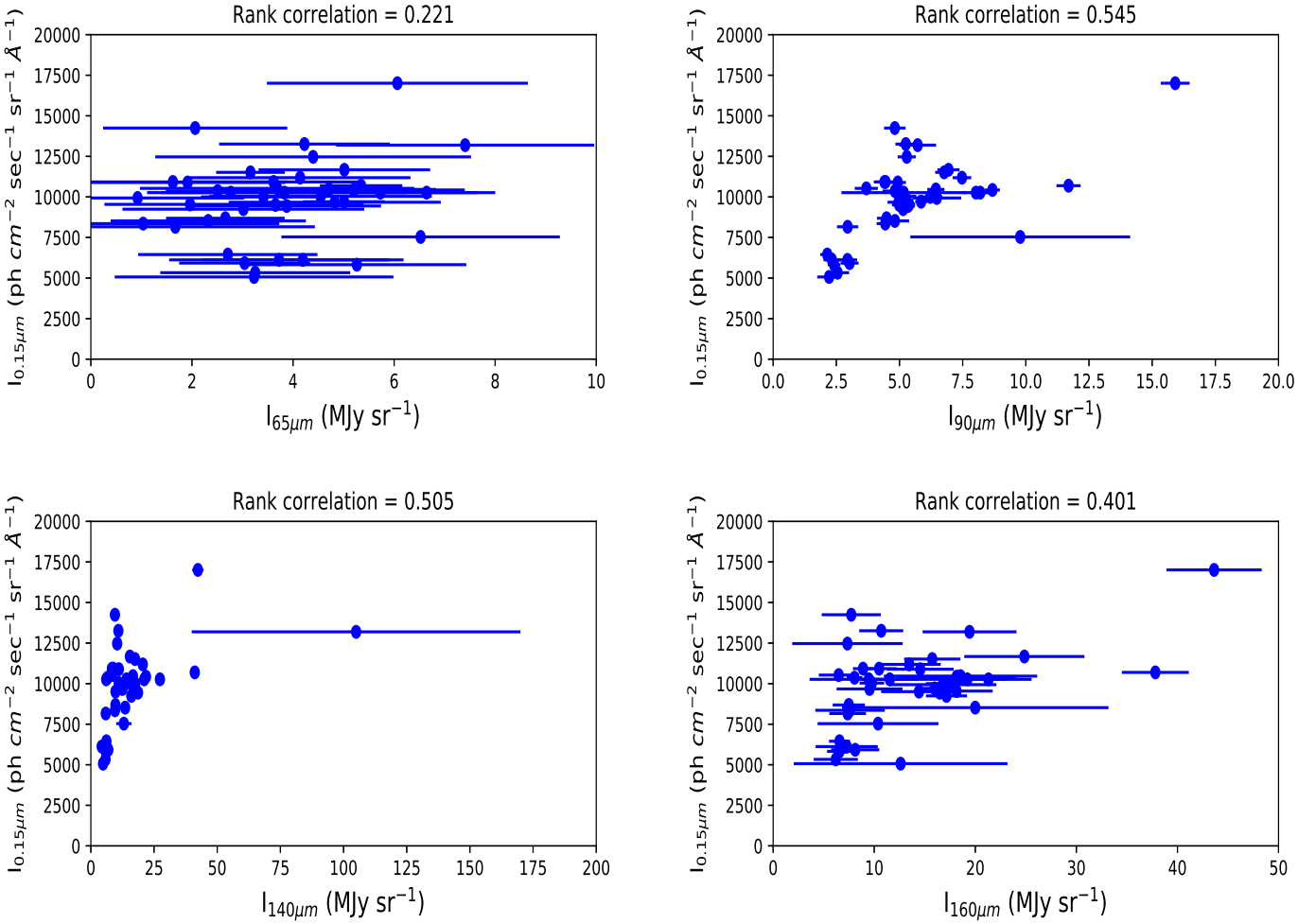

Figure 5.2: Correlation plots for the FUV-FIR intensities observed in Orion.

We have calculated the Spearman's rank correlations (ρ), as discussed in Section 1.3.2, among the FUV (1539 Å= 0.15 μm) and the four FIR wavelength intensities for which we have collected the archival data. The observed rank correlations between the *GALEX* FUV intensities from Table 5.2 and the AKARI FIR intensities from Table 5.3 are shown in Table 5.4 and the corresponding graphs are shown in Figure 5.2.

Table 5.4: The FUV-FIR rank correlations for 42 observed locations in Orion.

Wavelength	ρ	p-value
0.15 vs. 65 μm	0.221	0.1642
0.15 vs. 90 μm	0.545	0.0002
0.15 vs. 140 μm	0.505	0.0007
0.15 vs. 160 μm	0.401	0.0092

Our model gives the outputs separately for each combination of α, g and distance of dust cloud. We have done our calculations for a dust sheet 0.1 pc thick with input parameters as discussed in Section 5.3. We compare our model results with the observed *GALEX* FUV values from Table 5.2 by placing the dust at various distances ranging from 100 pc to 450 pc.

We obtain the best fit α, g and distance values for the different dust locations from our model and the results are presented in Table 5.5. Using the best fit distance values to each of the 42 individual dust locations, we are able to determine a 3D distribution of dust between us and the central Orion nebula region as shown in Figure 5.3.

Table 5.5: The best fit model parameters: albedo (α), asymmetry factor (g) and distance (d) at the 42 observed dust locations.

l (^{0})	b (^{0})	α	g	d (pc)
215.9858	-21.03678	0.7	0.6	221.7
216.3477	-20.05170	0.4	0.7	243.3
216.6843	-21.82404	0.4	0.6	168.9
216.3610	-22.73478	0.7	0.6	209.2
217.0416	-20.85384	0.9	0.6	297.6
217.3502	-19.92887	0.7	0.6	145.1
217.6604	-18.98852	0.6	0.6	127.3
203.7195	-26.30023	0.6	0.8	212.3
217.4199	-22.61161	0.6	0.4	160.5
217.7529	-21.67958	0.7	0.6	160.5
217.9658	-18.02852	0.5	0.9	124.5
217.0605	-23.54354	0.7	0.6	212.3
218.0538	-20.73285	0.8	0.0	127.5
203.1845	-26.43842	0.7	0.6	124.5
218.3820	-19.80989	0.7	0.6	183.1
200.9855	-24.76113	0.7	0.6	284.9
199.4499	-22.13578	0.7	0.6	293.2
199.0548	-19.42800	0.7	0.6	285.7
201.5206	-25.63027	0.7	0.6	302.1
218.2467	-17.08630	0.4	0.2	291.5
218.6914	-18.85640	0.7	0.7	268.8
198.9741	-21.24889	0.3	0.1	170.3
209.4986	-28.72108	0.3	0.2	218.3
210.6291	-28.62830	0.7	0.8	225.7
202.0663	-26.48617	0.7	0.6	232.5
218.4705	-22.45449	0.7	0.6	297.6
218.1448	-23.38423	0.7	0.6	243.9
217.7865	-24.31932	0.6	0.7	287.3
218.9770	-17.90198	0.9	0.1	310.5
218.5336	-16.11330	0.2	0.2	205.7
202.6347	-27.34658	0.1	0.5	177.3
199.3837	-23.90570	0.4	0.9	191.9
199.8962	-24.77457	0.6	0.3	228.3
219.4075	-19.65953	0.7	0.6	273.9
200.4167	-25.65025	0.4	0.0	266.6
203.5377	-10.56900	0.7	0.6	205.7
198.0511	-19.44966	0.7	0.6	135.8
219.2478	-16.95318	0.6	0.0	323.6
200.9614	-26.51945	0.7	0.6	250.6
209.0111	-29.63168	0.7	0.6	323.6
207.8586	-29.71661	0.7	0.6	392.1
201.5159	-27.37775	0.1	0.9	409.8

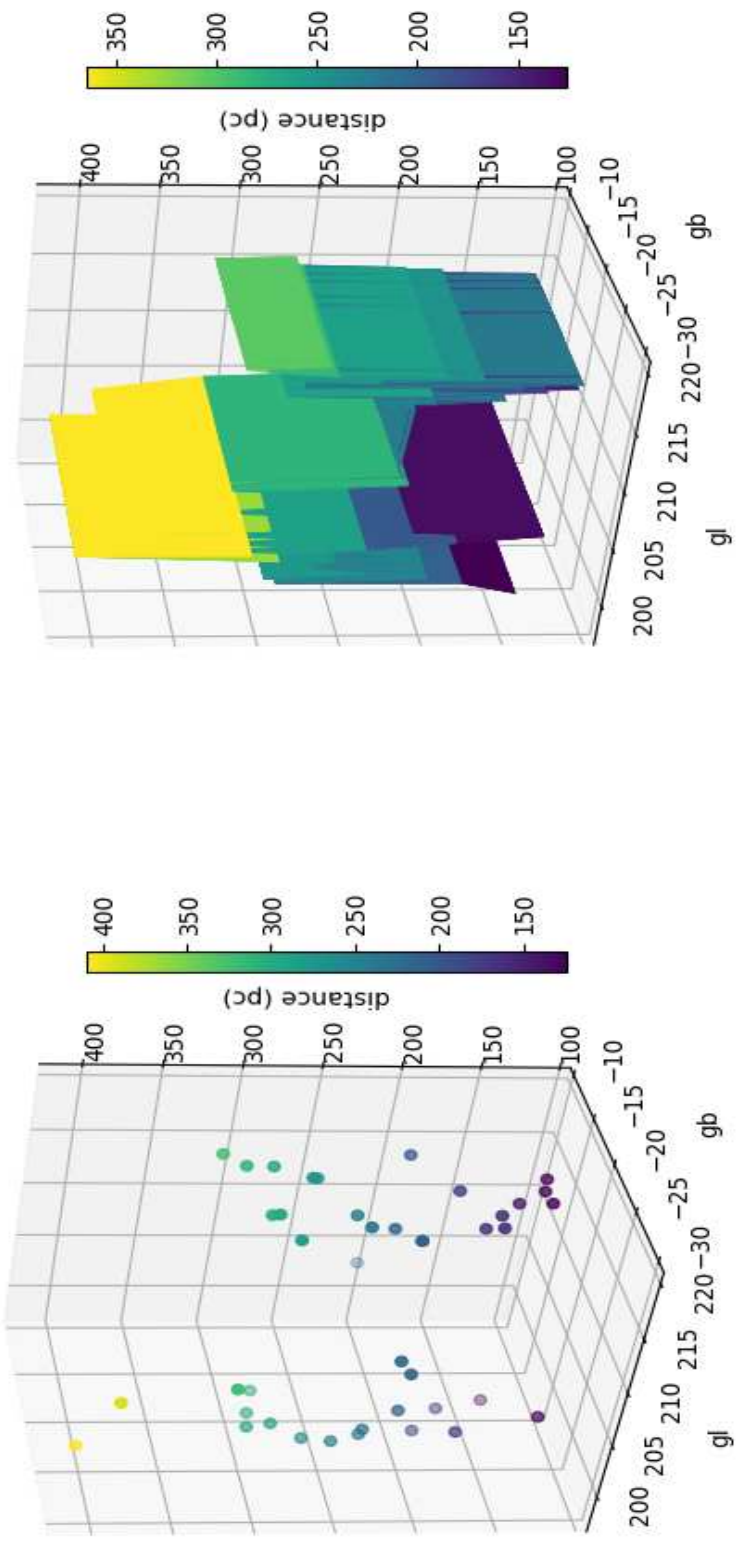

Figure 5.3: The distances to our dust locations shown as a 3D distribution on a scatter (left) and surface (right) plot.

5.5 Discussion and Conclusions

We see from our correlation studies in Table 5.4 and Figure 5.2 that the FUV–FIR rank correlation is almost similar for emission at 90 μm and 140 μm with a slightly weaker correlation coefficient at 160 μm. The correlation is more reliable for all longer wavelengths than what is seen at 65 μm due to the associated p-values. This shows that the dust species which shows emission at both wavelength bands around 100 μm is from similar cold environments [112–114]. The emission beyond 100 μm is from colder and even larger grains and hence the comparatively weaker correlation as we move to longer wavelengths. Nevertheless, the better correlation values at longer wavelengths indicate the origin of the emission to be from larger sized dust grains. This is in agreement to the recent findings of a lack of small dust particles in Orion as confirmed by the decrease in the strength of the 2175 Å feature [74].

The emission at 65 μm has been found to be associated with star-forming regions by Onaka & Okada (2003) [185] towards the Carina nebula. Hence, this might explain the observed low and unreliable value of correlation coefficient at FUV vs. 65 μm as the dust grains are prone to destruction in the presence of high UV radiation fields [147, 186]. The destruction of smaller dust grains might have occurred when it was in close vicinity to the central Orion region. The larger sized dust grains might have a better chance of survival and they are able to move away from the central region towards our observed locations. The overall correlation trend indicates that the dust contributing to the scattering in our locations away from the center of the Orion nebula is associated with colder environments as compared to the center which has the Trapezium star cluster. This is in agreement with the previous work done by Shalima et al. (2006) [89] where it was seen that dust in the neutral HI sheet (Orion's veil) is responsible for the scattering and not dust in the HII region. So this thin sheet of dust may be extending even for our observed locations but at a slightly different distance.

From our dust model, we see a higher deviation between the model and observed values as we move the dust farther away towards 450 pc from the distances specified in Table 5.5. Since the dust grains are forward scattering, it is expected that the dust responsible for the scattering should be in front of the stars which is evident from our distance calculations as shown in Figure 5.3. In order to check this argument, we have removed all the dust behind the stars to see the contribution from foreground dust. We find that the change in output varies from 0.4–16% which means that at least 84% of the light

scattering is from foreground dust. Schlafly et al. (2015) [181] have found a circular ring of dust engulfing the star-forming regions as well as dust clouds in Orion and they have estimated all the material to be lying between 400–550 pc giving a 150 pc depth and 100 pc width to the ring. Almost all of our dust locations lie within the 100–400 pc range (Table 5.5) and hence we are less concerned with the negligible background dust contaminating our observed results.

We have tried to check the results by grouping our locations into four regions according to their position in Figure 5.1. Group 1: single location on top of the 14 stars at the center, Group 2: 15 locations to the left, Group 3: 4 locations to the bottom, Group 4: 22 locations to the right of the central region. We see that there is a consistency for all the groups irrespective of the distance and location and although individual locations have varying α and g with distance (Table 5.5), each group has the same median values for these parameters, i.e. α=0.7, g=0.6 at 1539 Å. This is an increase in the value of the albedo from those observed by Shalima et al. (2006) [89] at lower wavelengths for their sample. This is also higher than the theoretically predicted value of α=0.4 by Draine (2003) [1] at similar wavelengths for average Milky Way dust with R_v=5.5. However, this is the median value for our locations and we do see a few individual locations in Table 5.5 with albedo values matching with the predictions of Draine (2003) [1].

In conclusion, we find the dust grains contributing to the extinction in our locations to be associated with colder environments as compared to the central Orion region (with the Trapezium star cluster) which agrees with the observations made by Shalima et al. (2006) [89], where Orion's veil is seen to be responsible for the scattering and not the HII region dust. We also see better correlation values at longer wavelengths indicating the origin of the emission to be from larger sized dust grains. We find the median values of dust optical properties from our model parameters to be α=0.7, g=0.6, which are the same for all four groups in Figure 5.1 irrespective of distance or location. This might be attributed to the presence of larger sized dust grains at our locations leading to high extinction values.